JACS
JOURNAL OF THE AMERICAN CHEMICAL SOCIETY

ARTICLE

pubs.acs.org/JACS

Hierarchical Self-Assembly of Semiconductor Functionalized Peptide α-Helices and Optoelectronic Properties

Rohan J. Kumar,*[,†] James M. MacDonald,[†] Th. Birendra Singh,[†] Lynne J. Waddington,[‡] and Andrew B. Holmes[†,§]

[†]CSIRO Materials Science and Engineering, Private Bag 10, Clayton South, Victoria 3169, Australia

[‡]CSIRO Materials Science and Engineering, 343 Royal Parade, Parkville, VIC 3052, Australia

[§]School of Chemistry, Bio21 Institute, University of Melbourne, VIC 3010, Australia

S Supporting Information

ABSTRACT: To determine the ability of semiconductors templated by α-helical polypeptides to form higher order structures and the charge carrier properties of the supramolecular assemblies, L-lysine was functionalized with a sexithiophene organic semiconductor unit via iterative Suzuki coupling and the click reaction. The resultant amino acid was incorporated into a homopolypeptide by ring-opening polymerization of an amino acid *N*-carboxyanhydride. Spectroscopic investigation of the polypeptide revealed that it adopted an α-helical secondary structure in organic solvents that underwent hierarchical self-assembly to form higher order structures. In cyclohexane, the polymer formed organogels at 2% (w/v). Organic photovoltaic and organic field effect transistor devices were fabricated by deposition of the PCBM blended active layer from chlorobenzene at concentrations shown to induce self-assembly of the polymer. Compared with control compounds, these devices showed significantly greater hole mobility, short circuit current, and efficiency. This work establishes the potential of this previously unreported bioinspired motif to increase device performance.

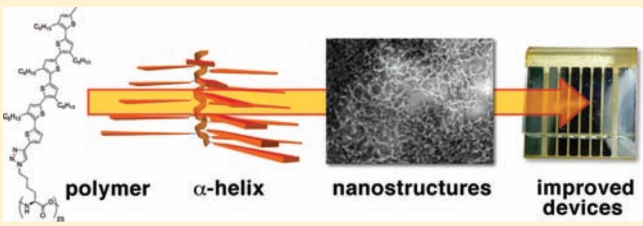

INTRODUCTION

Bottom-up molecular self-assembly,[1] in which the information for the correct hierarchical assembly of materials is encoded at a molecular level is an emerging technology that promises to have significant impact on manufacturing. Evolution has produced a vast array of conformational diversity and functionality from bottom-up molecular self-assembly based on the sequence information contained in a variety of biopolymers. Much attention has therefore focused on the rational design of self-assembled nanostructures using biopolymers such as DNA,[2] RNA,[3] and polypeptides.[4]

Recently, along with other modes of supramolecular organization,[5] such bioinspired approaches have found further application in the organization of π-conjugated oligomers.[6] A possible application of such research is in a variety of electronic devices that comprise a heterogeneous mixture of electron-donor (D) and electron-acceptor (A) materials. These devices are highly dependent upon feature sizes at the nanometer scale, resulting from control of the morphology of the constituent D and A materials.

Initial studies employing oligophenylenevinylenes and oligothiophenes with biological scaffolds including nucleobases,[7] carbohydrates,[8] steroids,[9] and peptides[10] have characterized the nanostructures formed and used the optical properties of such systems to monitor the self-assembly process.[11] Hybrid π-conjugated oligomer/peptide systems have focused primarily on amphiphilic peptide systems[10a,b] or the use of short amino acid segments selected for the propensity to form β-sheets, which are subsequently covalently attached to the π-conjugated chromophore.[10c−g] A limitation of these approaches may be the reduced charge transport properties of the materials due to the increased molar percentage of nonconducting material; however, this has not been investigated in the examples given.

A related approach using semiconductors attached to self-organizing amide substituents has recently been investigated.[12] It was observed that intermolecular hydrogen bonding promoted the formation of 3D organogels, which have been associated with increases in charge mobility as measured in organic field effect transistors[12a] (OFETs) and time-resolved microwave conductivity measurements.[12c]

α-Helical peptides synthesized by traditional peptide coupling techniques have been used in photophysical studies to investigate the degree of excitonic coupling between chromophores at different positions on the α-helix[13] and as bridges between chromophores in the study of photoinduced electron transfer.[14] Additionally, aromatic moieties templated by α-helical peptide homopolymers have been reported in the field of nonlinear optics.[15] There has been limited application of self-assembling peptide structures in organic photovoltaics (OPVs), with one study using a peptide 16-mer to template the supramolecular

Received: December 3, 2010
Published: May 13, 2011

interaction of porphyrins and fullerenes, resulting in increased device efficiency.[10i] However, the secondary structure and self-assembly properties of the peptide were not addressed. Additionally, the device configuration was not standard. It involved the electrophoretic deposition of porphyrin oligomers on nanostructured SnO_2 electrodes followed by supramolecular association of a fullerene. Another study employed the self-organization of amyloid fibrils to generate supramolecular order in a blend of semiconductor polymers and fullerenes.[16] Devices containing low concentrations of the amyloid fibrils demonstrated improved efficiency compared with control devices. Self-assembling, α-helical homopolypeptides bearing semiconducting groups have not been reported.

A prototypical α-helical peptide homopolymer is poly-γ-benzyl glutamate (PBLG), which exhibits a stable secondary structure in organic solvents due to the formation of hydrogen bonds.[17] These α-helices can then self-assemble in a hierarchical manner[18] to produce gel-forming 3D networks[19] of high dielectric constant.[18b] These properties seem to be ideally suited for application to organic bulk-heterojunction photovoltaic devices,[20] in which interdigitated and bicontinuous networks are required to ensure control of the critical electronic processes of charge separation and charge transport.[21]

In this study, the attachment of an oligothiophene derivative to the side chain of L-lysine and subsequent polymerization to the corresponding poly L-lysine derivative (**3**, Figure 1) are reported. The properties of the protected amino acid (**2**), the polymer (**3**), and a related achiral sexithiophene (**1**) were investigated. The polymer (**3**) formed an α-helical secondary structure (as evidenced by IR and NMR spectrometry), which underwent hierarchical self-assembly in a variety of solvents. Furthermore, the control of supramolecular organization resulted in improved photovoltaic and OFET device properties observed for the polymer (**3**) compared with the control systems (**1**, **2**).

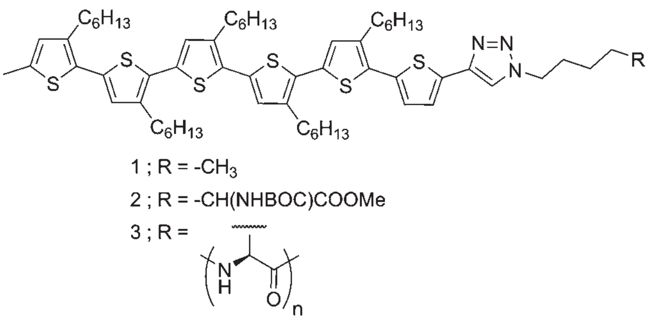

Figure 1. Structures of **1**−**3**.

■ SYNTHESIS

A convergent approach was adopted for the synthesis for the target sexithiophene-functionalized L-lysine monomer (**2**). Initially, an α-alkynyl terthiophene fragment (**8**) was prepared by iterative Suzuki coupling of 2-(3-hexylthiophen-2-yl)-4,4,5,5-tetramethyl-1,3,2-dioxaborolane (**4**) to the commercially available 5-bromo-2-carbaldehyde (**5**) followed by bromination of the newly incorporated thiophene with *N*-bromosuccinimide (NBS). The aldehyde (**8**) was then converted into the terminal alkyne (**10**) via Corey−Fuchs methodology (Scheme 1).[22] The alkyne (**8**) is moderately unstable at ambient conditions and must be stored at low temperature under inert atmosphere.

The α-alkynyl terthiophene (**10**) served as a synthon for the copper-catalyzed variant of the Huisgen triazole formation (Scheme 2).[23] The pentyl derivative (**11**) was accessed via a one pot, two-step procedure as reported by Hawker and coworkers,[24] whereas the L-lysine sexithiophene derivative (**13**) was obtained via reaction with (*S*)-6-azido-2-(*tert*-butoxycarbonylamino)hexanoic acid. The terminal thiophene rings of the products **11** and **14** were then iodinated for use in a Suzuki coupling to incorporate the second terthiophene fragment.

The second terthiophene fragment (**23**) was synthesized via a similar iterative Suzuki coupling approach as was used for the synthesis of the alkyne **10**. 2-Bromo-3-hexyl-5-methylthiophene (**18**) was prepared by a two-step procedure from 3-hexylthiophene (**16**, Scheme 3). Potential reaction at the 5-position of the terminal thiophene unit was suppressed by introduction of a methyl substituent using lithium 2,2,6,6-tetramethylpiperidine (LiTMPP) selectively to deprotonate the less hindered α-position, as described by Smith and Barratt.[25] The boronate ester (2-(4-hexylthiophen-2-yl)-4,4,5,5-tetramethyl-1,3,2-dioxaborolane, **19**) was prepared by a similar deprotonation and boronation at the less hindered position. This molecule was used in the subsequent coupling.

The sexithiophene compounds (**1**−**3**) were prepared by a final Suzuki coupling reaction (Scheme 4). It was intended to form the polypeptide (**3**) by ring-opening polymerization of the *N*-carboxyanhydride (**25**), which was prepared by saponification of the ester (**2**) and cyclization of the corresponding carboxylic acid (**24**) with triphosgene. The amphiphilic nature of the cyclic

Scheme 1. Synthesis of 5-Ethynyl-(3′,3″-hexyl-2,2′:5′2″-terthiophene) 10[a]

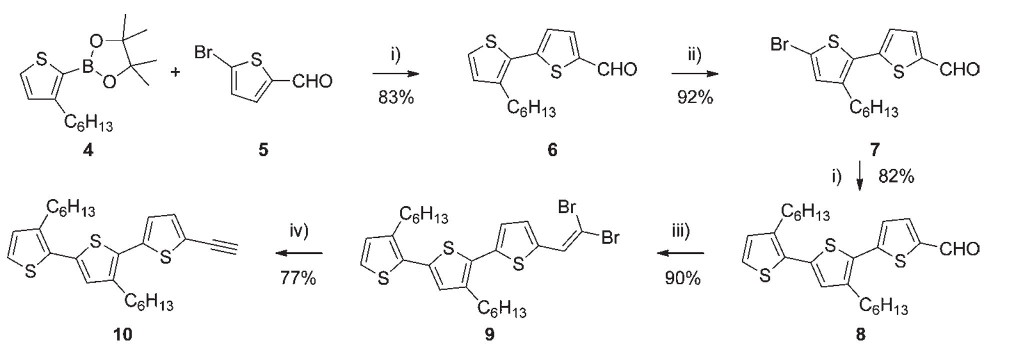

[a] Reagents and conditions: (i) $Pd(PPh_3)_4$, Cs_2CO_3, toluene, reflux, 16 h; (ii) NBS, AcOH, $CHCl_3$, 0 °C to room temperature, 2 h; (iii) CBr_4, PPh_3, CH_2Cl_2, 0 °C to room temperature, 1 h; (iv) *n*-BuLi, THF, −78 °C, 3 h.

dx.doi.org/10.1021/ja110858k |*J. Am. Chem. Soc.* 2011, 133, 8564–8573

Scheme 2. Formation of Triazole (11 and 13) and Subsequent Halogenation[a]

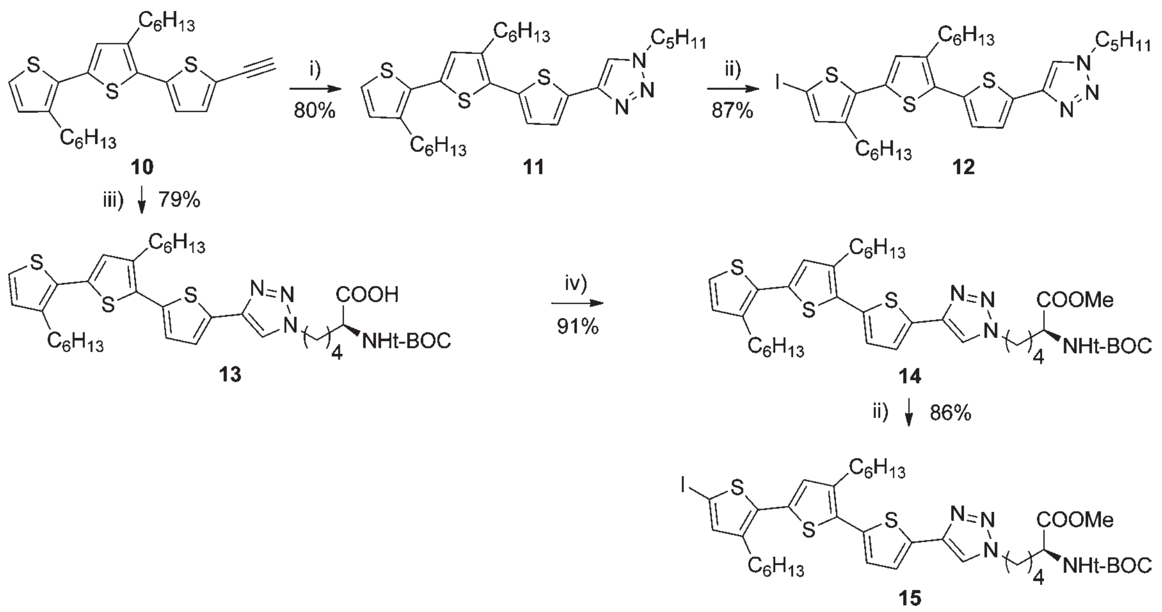

[a] Reagents and conditions: (i) 1-bromopentane, NaN_3, sodium ascorbate, $CuSO_4 \cdot 5H_2O$, DMF, 70 °C, 16 h; (ii) *N*-iodosuccinimide, AcOH, $CHCl_3$, 0 °C to room temperature, 2 h; (iii) (*S*)-6-azido-2-(*tert*-butoxycarbonylamino)hexanoic acid, sodium ascorbate, $CuSO_4 \cdot 5H_2O$, H_2O, *n*-BuOH, room temperature, 16 h; (iv) K_2CO_3, MeI, DMF, 0 °C to room temperature, 16 h.

Scheme 3. Complementary Terthiophene Synthesis[a]

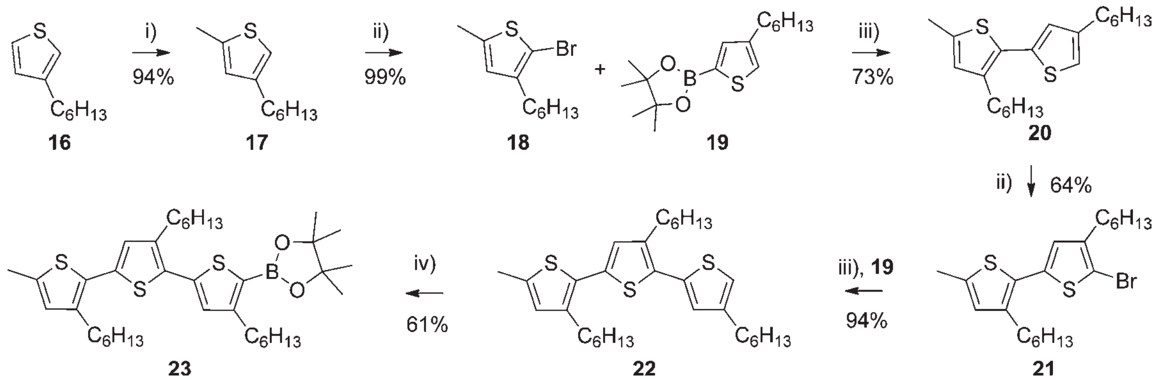

[a] Reagents and conditions: (i) (a) 2,2,6,6-tetramethylpiperidine, *n*-BuLi, −78 °C, 1 h then (b) **16**, −78 °C, 1 h then (c) MeI, −78 °C to room temperature, 2 h; (ii) NBS, AcOH, $CHCl_3$, 0 °C, 2 h; (iii) $Pd(PPh_3)_4$, Cs_2CO_3, toluene, reflux, 16 h; (iv) *n*-BuLi, 2-isopropoxy-4,4,5,5-tetramethyl-1,3,2-dioxaborolane, −78 °C, 2 h, room temperature, 16 h.

anhydride limited its solubility in common solvents, allowing NMR characterization only at low concentration in DMSO at 50 °C. Additionally, attempts at purification by chromatography[26] or recrystallization resulted in decomposition. The products of the anhydride formation were CO_2 and $Et_3N \cdot HCl$, and the bulk of the latter was removed by the filtration of the crude product in cold anhydrous THF; however, batch to batch variation in the level of this impurity was observed.

Ring-opening polymerization of the anhydride **25** was then carried out, using the hexamethyldisilazane (HMDS)-initiated method reported by Lu and Cheng.[27] At 1 mol % initiator concentration, polymerization could not be initiated and the starting anhydride remained in solution. At higher concentrations of initiator (5−10 mol %), polymerization was initiated and its progress could be monitored by FTIR spectroscopy. The diagnostic signals in the IR spectra were the anhydride signal (1785 cm^{-1}) that decreased, and the amide carbonyl stretching frequencies (1660 cm^{-1}) that increased. Typically, for 10 mol % initiator concentration a molecular weight of 23 kg/mol (n = 23, polydispersity index = 1.1) was obtained as measured by GPC against a polystyrene standard. This degree of polymerization was higher than was calculated from the initiator to monomer ratio that was used. This may indicate the interaction of the initiator in solution with an impurity present in the starting material. However, the excellent polydispersities obtained (1.05−1.3) indicate that the polymerization was essentially living. Given the difficulties in purification of the starting material, no further attempt was made to investigate the higher than expected molar mass of the polymer. A single polymer batch, purified via size exclusion chromatography and subsequent

Scheme 4. Synthesis of Sexithiophene Compounds[a]

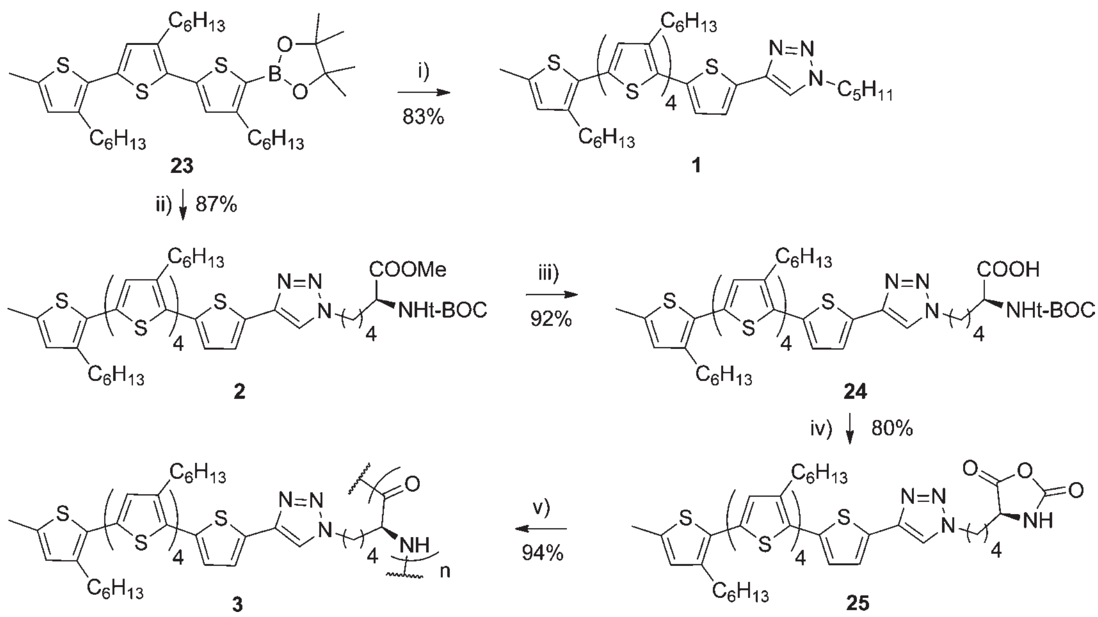

[a] Reagents and conditions: (i) **12**, $Pd(PPh_3)_4$, K_2CO_3, DME, H_2O, 130 °C MW, 1 h; (ii) **15**, $Pd(PPh_3)_4$, Cs_2CO_3, toluene, reflux, 16 h; (iii) LiOH, THF, H_2O; (iv) Et_3N, triphosgene, EtOAc; (v) HMDS, THF, 32 h.

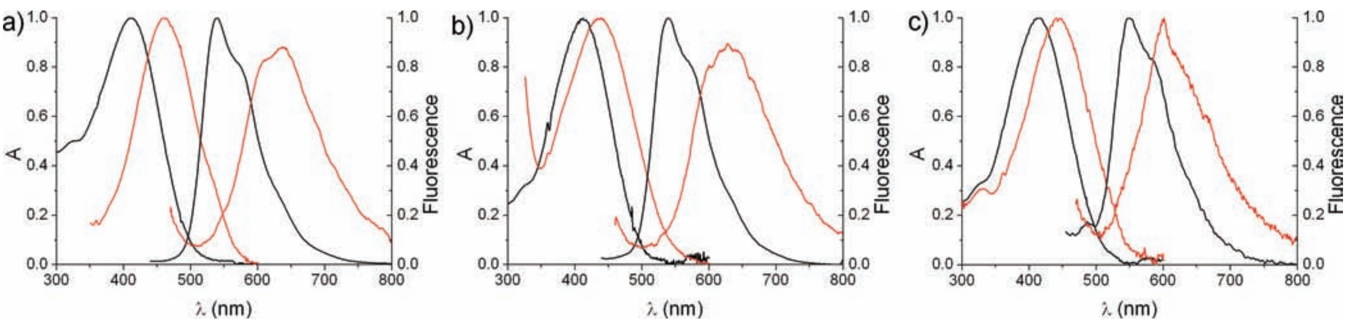

Figure 2. Normalized absorption and fluorescence spectra in $CHCl_3$ at 2.1×10^{-7} M (black) and thin film (red) for a) **1**, b) **2**, and c) **3**.

precipitation, resulting in a sample of approximately 23 repeat units in length (as estimated by GPC) that was used in all subsequent characterization.

OPTOELECTRONIC CHARACTERIZATION OF 1−3

UV−vis absorption spectroscopy of **1**−**3** in $CHCl_3$ (Figure 2) shows a large peak at 415 nm that was assigned to the $\pi-\pi^*$ transition of the oligothiophene. Very little difference was seen between the λ_{max} of the compounds indicating the chromophores have a similar conformation and solvation. Similarly, the fluorescence emission spectra was similar for **1**−**3**, displaying the characteristic vibronic fine structure observed in oligothiophenes due to the increase of planarization of the excited state.[8] The similarity of the absorption and emission spectra of **1**−**3** indicates that there is very little intramolecular interaction between the chromophores for **3** in chloroform. Upon spin-casting neat films of **1**−**3** from chlorobenzene onto glass, all compounds showed a bathochromic shift of their absorption spectra along with a narrowing of the absorption band, which may arise from the increased planarization of the chromophores in the solid state[28] or from the formation of J-aggregates.[12a] Compound **1** showed a shift of 45 nm, larger than that of **2** and **3** (∼24 nm), indicating that **1** has an increased degree of planarization or J-aggregate character, presumably due to the lack of steric bulk attached to the triazole that would disrupt stacking.

The electrochemical properties of **1**−**3** were studied by cyclic voltametry in CH_2Cl_2 and showed two reversible oxidation peaks (Table 1); however, no reduction peak was observed inside the solvent window. The position of the HOMO in spin-cast films of **1**−**3** was determined by photoelectron spectroscopy in air (PESA).[29] In the absence of electrochemical data regarding reduction potential of the compounds, the LUMO levels were determined from the PESA-determined HOMO and the subtraction of the HOMO−LUMO energy as estimated by the film absorption onset.

SELF-ASSEMBLY

FTIR analysis of a thin film of polymer **3** exhibited a carbonyl stretching (amide II) band at 1654 cm^{-1} and an N−H bending (amide I) band at 1547 cm^{-1} (part a of Figure 3). These are

Table 1. Electrochemical Data for 1 − 3

compound	$E_{1/2}$[a] (ΔE_p)[b] R^+/R	$E_{1/2}$[a] (ΔE_p)[b] R^{2+}/R^+	E_{onset}[c]	HOMO (eV)[d]	E_g (eV)[e]	LUMO (eV)
1	0.29 (0.19)	0.46 (0.19)	0.178	−4.97 (−4.87)	2.08	−2.79
2	0.30 (0.17)	0.44 (0.19)	0.201	−5.05 (−5.17)	2.20	−2.97
3	0.29 (0.18)	0.50 (0.11)	0.110	−4.91 (−5.01)	2.20	−2.81

[a] Half wave potential determined as the average of the anodic and cathodic peak potentials, V vs ferrocene 10 mM in CH_2Cl_2, 0.1 M $Bu_4N(PF_6)$. [b] Difference between the anodic and cathodic peak potentials, V, ν = 0.1 mV s^{-1}. [c] Estimated from the onset of absorption in thin films. [d] Determined from $E_{HOMO} = -(E_{ox}^{onset} + 4.80)$ eV,[30] data in brackets measured by PESA on thin films. [e] $E_{LUMO} = E_{HOMO} + E_g$.

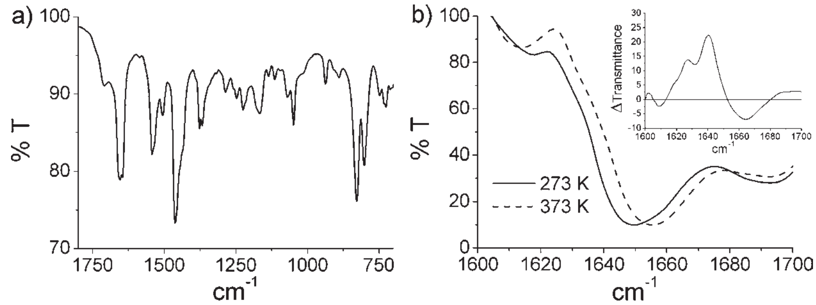

Figure 3. a) FTIR spectrum of a film of compound **3**, b) shift of amide II band position (solvent corrected) in chlorobenzene at 273 and 373 K (difference spectra insert).

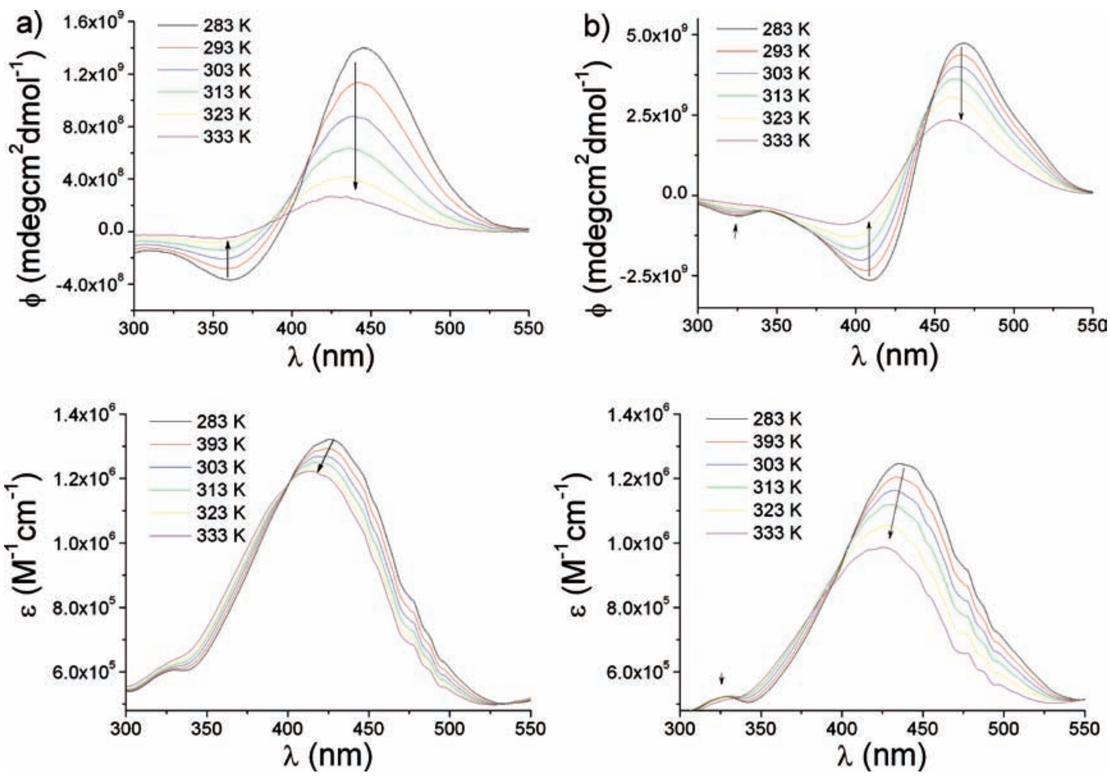

Figure 4. Variation of CD spectra and corresponding absorption spectra (below) with increasing temperature of **3** at 2.1 × 10^{-5} M in a) chlorobenzene, b) chloroform, and c) cyclohexane.

characteristic of α-helical secondary structure, in keeping with observations for rigid, α-helical amino acid homopolymers.[18b] Helical stability has been shown to be dependent on polymer length with short oligomers of PBLG having been shown to adopt *β*-sheet structures with a characteristic carbonyl stretching at 1625 cm^{-1}.[18b] No signal was observed at this wavenumber for **3** indicating a predominantly α-helical structure in a film. In chlorobenzene at ambient temperature, the solvent corrected IR

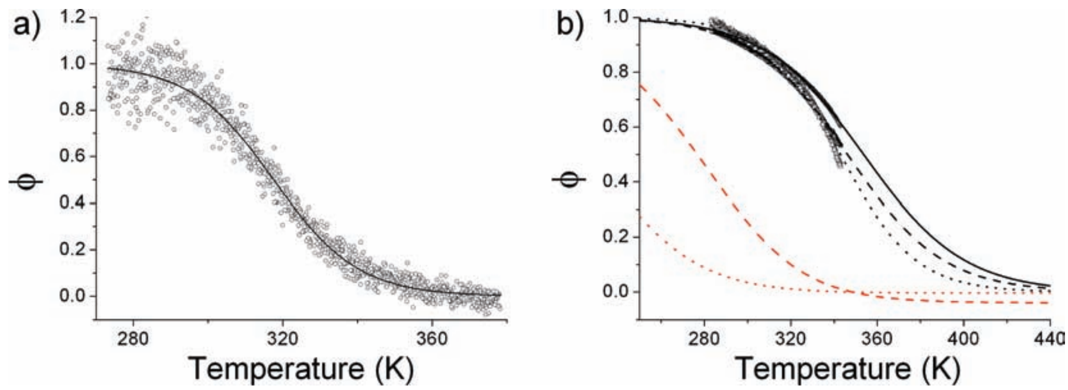

Figure 5. Temperature dependence of the normalized CD spectra (ϕ) as a function of temperature in a) chlorobenzene at 4.6 × 10^{-5} M and b) cyclohexane at 2.1 × 10^{-5} M (black solid line), 2.1 × 10^{-6} M (black dashed line), and 2.1 × 10^{-7} M (black dotted line). Additionally, the predicted curves calculated from a numerical solution from eq 2 are shown for 2.1 × 10^{-6} M (red dashed line) and 2.1 × 10^{-7} M (red dotted line).

spectrum displays an amide II band that is characteristic of α-helical secondary structure with a peak centered 1649 cm^{-1} (part b of Figure 3). It exhibits a small shift to higher wavenumber when heated to 373 K. The difference spectra of the two components show a negative component at 1664 cm^{-1} and a positive component at 1640 cm^{-1} associated with an increase in the random coil and a reduction in α-helical content respectively.[31]

The ^{1}H chemical shift of the α-proton of the polypeptide backbone is diagnostic of secondary structure in α-helical homopolypeptides.[32] In deuterated chlorobenzene, this chemical shift was not easily observed due to it lying coincident to that of the protons α to the triazole. The amide proton is known to be less diagnostic than the peptide α-proton of changes in secondary conformation of amides.[33] For **3** at 274 K, a single broad peak is observed, upon heating to 373 K, two upfield shifted resonances are observed (Supporting Information). These can be interpreted as the shifts for two populations of hydrogen-bonded amide protons with different bond lengths or those associated with the α-helical and random coil conformations. Taken together with the IR data, this indicates unfolding of the α-helical structure at 373 K in chlorobenzene.

Circular dichroism (CD) spectroscopy provides further evidence for the secondary structure formation of **3**. Compounds **1** and **2** showed no CD spectra at the concentrations studied (2.1 × 10^{-5} M). In contrast, the CD spectra of **3** in chlorobenzene and cyclohexane at room temperature showed a bisignate signal (Figure 4), with the zero crossing at the absorption λ-max of the oligothiophene. These observed CD spectra are not artifacts arising from linear dichroism of higher order structures (Supporting Information) but are rather assigned as the excitonic coupling between chromophores. The observed Cotton effect may arise due to intrahelical excitonic coupling of pendant chromophores[34] or due to an interhelical self-assembly process leading to higher order structures. This was investigated further by variable temperature CD spectroscopy in chlorobenzene and cyclohexane.

The CD spectra and the associated absorption spectra show that the Cotton effect increases with decreasing temperature and that this is associated with an increase in absorption and a bathochromic shift of the $\pi-\pi^*$ transition (Figure 4). The observed shift in λ-max is from 426 nm (283 K) to 414 nm (333 K) in chlorobenzene and from 436 nm (283 K) to 423 nm (333 K) in cyclohexane. Additionally, the changes to the $\pi-\pi^*$ transition with temperature can be seen to pass through an isosbestic point and are accompanied by a small, new feature at 325 nm. This can be interpreted as the simultaneous presence of H- and J-aggregates, as observed by Stupp and co-workers in self-assembling sexithiophenes,[12a] or a two-state thermochromic rearrangement of the chromophore as previously observed in polythiophenes.[35] This is a topic for continued investigation.

The intensity of the CD spectra is inversely related to the temperature for both solvent systems investigated. In order to establish how CD intensity varies as a function of temperature, the temperature was varied at a rate of 0.5 K/min, whereas the CD signal was recorded at 445 nm in chlorobenzene (part a of Figure 5) and 468 nm in cyclohexane (part b of Figure 5). At this rate, the transition exhibited no hysteresis and no difference was seen in the trace by performing the experiment at a reduced scan rate (0.2 K/min, Supporting Information).

The CD signal varies in a sigmoid fashion with temperature in chlorobenzene, which can be approximated as a two-state equilibrium, fitted using a Boltzmann function, and subsequently normalized. In cyclohexane, the entire transition is not observed, however the data can be fitted using a Boltzmann function imposing the lower boundary constraint of 0, assuming that the degree of excitonic coupling will reach 0. Such sigmoid temperature dependence of CD data has previously been used to describe both the intramolecular helix–coil transition[31] and intermolecular self-assembly.[36] In order to determine the origin of the temperature dependent CD spectra, data was collected over a concentration range of 3 orders of magnitude in cyclohexane. An intramolecular process is expected to have a temperature dependent equilibrium constant (K_e) that is independent of concentration and related to the normalized degree of helical content (ϕ) as expressed by eq 1. In contrast, an intermolecular aggregation process is expected to be concentration dependent, as quantified by Meijer and co-workers for isodesmic (two-state) systems using eq 2, where ϕ is the degree of aggregation, K_e the equilibrium constant and c_T the total concentration of molecules.[36]

$$K_e = \frac{\phi}{(1-\phi)} \tag{1}$$

$$\frac{1}{\sqrt{1-\phi}} = \frac{1}{2} + \frac{1}{2}\sqrt{4K_e c_T + 1} \tag{2}$$

The experimental data in part b of Figure 5 (black lines) shows little concentration dependence and no relationship to the curves

dx.doi.org/10.1021/ja110858k |J. Am. Chem. Soc. 2011, 133, 8564–8573

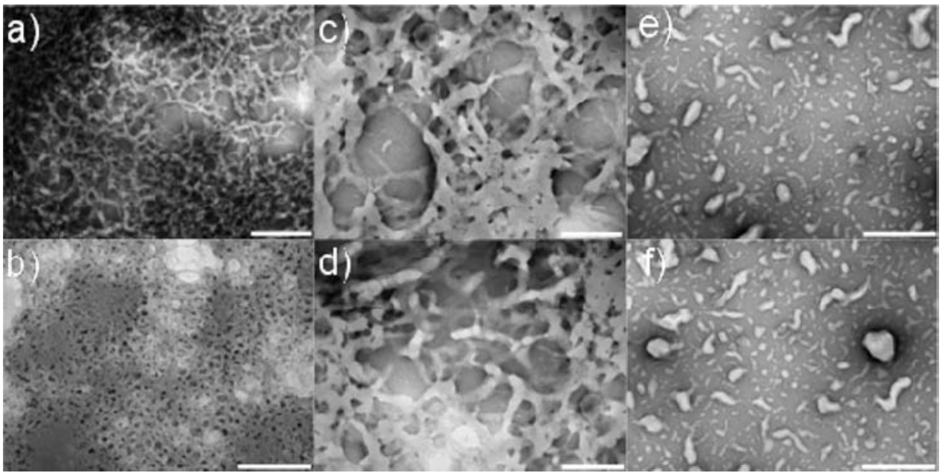

Figure 6. Self-organization of polymer **3**, as visualized by negative staining (uranyl acetate in EtOH) TEM of samples deposited from solutions of **3** in cyclohexane. (a)−(d) 2.1×10^{-5} M; (e) and (f) 1.0×10^{-5} M. Scale bar (a), (b): 500 nm; (c), (d): 200 nm; (e), (f): 500 nm.

generated from a numerical solution of eq 2 (red lines in part b of Figure 5) based on the equilibrium constants calculated at the highest concentration. Thus, the excitonic coupling arises from an intramolecular process that is related to helical unfolding. The slow helical unfolding over a large temperature range is in keeping with similar observations in other polypeptides.[37] On the basis of the degree of excitonic coupling observed at ambient temperature in cyclohexane and chlorobenzene, it is possible to estimate the fraction of residues in the helical conformation as 0.95 and 0.89 respectively at 293 K. A van't Hoff plot (Supporting Information) was generated using the using eq 1 and the data shown in Figure 5 allowing the thermodynamic parameters of α-helix formation to be calculated as ΔH equal to −509 J/mol and ΔS equal to −1.42 J/mol.

To determine if the α-helical structures could undergo intermolecular self-assembly, the solubility and organogel-forming properties of **1**−**3** were investigated in a variety of organic solvents (Supporting Information). The formation of an organogel, a good macroscopic indicator of nanostructure formation, was observed only for **3** in cyclohexane at 2% (w/v) concentration.

Dynamic light scattering (DLS) studies in chlorobenzene and chloroform at 2.1×10^{-5} M produced correlation curves (Supporting Information) that demonstrate that the average size of species in solution decreases with increased temperature. Chlorobenzene was found to contain smaller species in solution than cyclohexane at any given temperature and concentration. This gives a qualitative observation of self-assembly in solution at concentrations comparable with the spectroscopic measurements. However, given the polydisperse nature of the species in solution, quantification of the hydrodynamic radius of the species was not appropriate.

To directly visualize any nanostructures present, transmission electron microscopy (TEM) was employed. Highly branched nanostructures were observed to be deposited upon carbon coated copper grids from 2.1×10^{-5} M solutions of **3** in cyclohexane at room temperature (parts a−d of Figure 6). The morphology of these branched structures varied across the grid, in some areas forming a dense, spongelike material (part b of Figure 6) and in other areas forming more loosely interwoven networks (part d of Figure 6). In addition, occasional separate rodlike structures are observed (part c of Figure 6) indicating that the network may form from the outward growth and subsequent enmeshing of smaller nucleating particles. At a concentration of 1.0×10^{-5} M of **3** in cyclohexane, smaller rodlike or globular nanoparticles predominated and, only occasionally becoming associated in a loose and diffuse network, were observed illustrating the concentration dependent nature of the self-assembly (parts e and f of Figure 6).

Samples for TEM were also prepared from 2.1×10^{-5} M of **3** in chlorobenzene. Results obtained were similar to those obtained for cyclohexane (Supporting Information) with nanoparticles present, which were seen to be associated into branched networks. The highly branched meshlike networks observed for cyclohexane were not observed in chlorobenzene at the same concentration indicating that self-assembly is more favorable in cyclohexane than chlorobenzene, as observed via DLS.

Compounds exhibiting hierarchical self-assembly from α-helical secondary structures have been studied extensively, with support for both an isodesmic mechanism based on spinodal decomposition of isotropic solutions[19] and a nucleation−growth mechanism.[18a] The TEM data for polymer **3** clearly indicate a branched morphology of the nanostructures observed by TEM in keeping with observations for other α-helical homopolypeptides. In terms of the application to organic solar cells, this may prove a useful form of nanostructure to achieve interpenetrating D−A networks, which are widely thought to be the optimal morphology for these devices. No evidence is seen in the TEM data for elongated fibers often observed in nucleation−growth type self-assembly processes.[11c] It is interesting to note that the solvent in which a more stable helix is observed results in more extensive nanostructures, as observed by TEM, although the causality of this relationship has not been established. It is proposed the self-assembly process consists of the initial formation of an α-helical secondary structure followed by intermolecular association based on van der Waals and $\pi-\pi$ stacking interactions which result in the observed higher order structures.

■ DEVICE MEASUREMENTS

Solution processed bulk heterojunction devices containing **1**−**3** with phenyl-C_{60}-butyric acid methyl ester (PCBM) as D−A blends in the active layer were fabricated to investigate the potential of the observed self-assembly when translated to the solid phase to enhance photovoltaic efficiency. The calculated

Table 2. OPV Device Performance[a]

compound	J_{sc}[b] (mA/cm^2)	V_{oc}[c] (V)	FF[d]	η[e] (%)
1[f] (n = 11)	0.91 ± 0.013	0.53 ± 0.073	27.8 ± 0.47	0.14 ± 0.018
2[g] (n = 7)	0.76 ± 0.011	0.59 ± 0.025	26.3 ± 0.48	0.12 ± 0.007
3[h] (n = 11)	1.30 ± 0.051	0.61 ± 0.031	27.7 ± 0.75	0.22 ± 0.017
P3HT[i] (n = 12)	4.74 ± 0.19	0.70 ± 0.004	37.1 ± 0.67	1.24 ± 0.005

[a] Data are mean ± standard deviation for the number of devices shown (n). Characteristics of photovoltaic devices made from 1:2 molar ratio blends of **1**−**3** with PCBM at the concentrations shown. The active layer was deposited by spin-coating from chlorobenzene. [b] Short circuit current. [c] Open circuit voltage. [d] Fill factor. [e] Device efficiency. [f] 9.4 mM **1**, 19.7 mM PCBM, 100 ± 4 nm. [g] 9.7 mM **2**, 19.8 mM PCBM, 102 ± 3 nm. [h] 10.5 mM **3**, 21 mM PCBM, 102 ± 3 nm. [i] P3HT/PCBM = 1:1 (w/w), 3000 rpm.

HOMO and LUMO levels (Table 1) indicate sufficient driving force for photoinduced electron transfer to PCBM (>0.3 eV). The architecture of the devices was glass/indium tin oxide/poly(3,4-ethylenedioxythiophene)poly(styrenesulfonate)/active layer/Ca/Al (Supporting Information for fabrication protocols). The active layer was deposited by spin coating films from solutions of chlorobenzene at the concentrations indicated (Table 2). The devices were not annealed to allow observation of the effects of self-assembly during deposition and this is the origin of the lower than usually reported performance for the benchmark P3HT/PCBM devices. Devices were made at a number of ratios of **1**−**3** to PCBM (Supporting Information) and overall device efficiency and the short circuit current was seen to increase with increasing PCBM content for all compounds. This indicates a low intrinsic charge mobility of the various donor materials. Devices comprising of a 1:2 molar ratio of D to A were chosen for comparison as these showed suitable film forming characteristics for reproducible device fabrication and contained a large enough fraction of D material to be representative of the D materials properties.

The data was subjected to one way ANOVA testing with Bonferroni means testing to determine the statistical significance of the observed differences. The obtained device efficiencies (η) show that the optimized devices containing **3** in the active layer are significantly more efficient than those containing **1** (p < 0.001) or **2** (p < 0.001). There was a nonsignificant difference between the efficiency of devices containing **1** and **2** (p = 0.11). The observed difference in efficiency is attributed to the significant increase in J_{sc} observed for compound **3** in comparison with both **1** (p < 0.001) and **2** (p < 0.001). This indicates that the helical arrangement of chromophores and subsequent hierarchical self-assembly results in more favorable domains for charge transport as J_{sc} is a parameter known to be affected by morphological characteristics of the active layer that influence charge transport.[16,38] Compound **1** had a significantly higher J_{sc} than **2** (p < 0.001) indicating the unfavorable morphological effects of the large carbamate group for **2**. The differences observed in V_{oc} for all compounds were largely insignificant; however, the lower V_{oc} observed for **1** may be a result of its low melting point and poor film forming qualities. The observed fill factors were low for all compounds. No significant difference was seen between **1** and **3** (p = 1) but the fill factor for **2** was significantly lower than both **1** (p < 0.001) and **3** (p < 0.001).

It is important to note that the concentrations of **3** used in the device fabrication were significantly higher than those used in the TEM experiments, which would lead to a higher degree of self-association and higher order structures, and these may be the physical basis of the improved solar cell performance. Confounding this effect is the presence of PCBM in the solution, which has an unknown effect on the self-assembly of **3**. AFM was thus employed to evaluate the morphology of the films (Supporting Information). The AFM images show that films made from **1** and **2** with PCBM give very smooth films with little observable crystalline features. In contrast, films from **3** show the presence of nanometer size protrusions from the surface, which may arise from the observed self-assembly of **3** into higher order structures.

Table 3. OFET Device Performance[a]

compound	μ_{hole} (cm^2/(V s))	$\mu_{electron}$ (cm^2/(V s))
1[b]	not active	7.4×10^{-4}
2[c]	not active	2.8×10^{-5}
3[d]	1.9×10^{-7}	5.2×10^{-6}

[a] Characteristics of OFET devices made from 1:2 molar ratio blends of compounds **1** − **3** with PCBM at the concentrations shown. The active layer was deposited by spin-coating from chlorobenzene. [b] 9.4 mM **1**, 19.7 mM PCBM, 3000 rpm. [c] 9.7 mM **2**, 19.8 mM PCBM, 3000 rpm. [d] 10.5 mM **3**, 21 mM PCBM, 3000 rpm.

To further explore charge transport effects and extract mobilities, OFET devices were fabricated using 1:2 blends of **1**−**3** with PCBM, as investigated in OPV devices. Bottom-gate, bottom-contact OFET devices were fabricated by spin coating blend solutions onto lithographically patterned, HMDS treated substrates and the extracted charge mobilities are shown in Table 3 (Supporting Information for current−voltage data).

The electron mobility, which will be primarily dependent on the existence of interpenetrating networks of PCBM, follows the trend **1** > **2** > **3**. Hole mobilities were too low to allow meaningful fitting of the OFET data for **1** and **2**. Compound **3** however showed a hole mobility in the order of 10^{-7} cm^2/(V s), which is at least an order of magnitude greater that that of **1** and **2** (mobilities of 10^{-8} cm^2/(V s) are measurable). Similarly, Stupp and co-workers observed higher hole mobilities in self-assembling sexithiophenes when cast from assembly promoting solvents compared with molecularly solvating solvents.[12a] The self-assembly of **3** may result in greater interpenetrating networks of p-type material, while simultaneously disrupting the n-type (PCBM) networks, leading to an increase in hole mobility and a decrease in electron mobility compared to the control devices, as observed. The increased hole mobility and greater balance of charge transport explain the increased photovoltaic device performance observed for **3**.

The p-type chromophores chosen in this study all have low performance in comparison with P3HT both in terms of performance in photovoltaic devices and charge mobility in OFETS. This is most likely due to a combination of effects including the greater absorption of P3HT in the visible region and favorable morphology of P3HT due to its crystallinity. The full potential of the use of peptide-based α-helical scaffolds is currently under investigation in our laboratories through the use of a modular approach, which will allow the incorporation of different small molecule dyes to enable both greater coverage of the solar spectrum and assessment of the differing morphologies accessible by this motif.

■ CONCLUSIONS

Polypeptide **3** was synthesized using iterative Suzuki coupling, click chemistry, and a living ring-opening polymerization.

Polypeptide **3** forms an α-helical secondary structure in organic solvents. This α-helical structure self-assembles into nanostructures. Solutions of a suitable concentration to exhibit the observed hierarchical self-assembly were blended with PCBM and used to construct OPV and OFET devices. The OPV devices showed enhanced efficiency and short circuit current in comparison with two reference compounds and the OFET devices exhibited enhanced hole mobility along with more balanced charge transport. All observations indicate that self-assembly of α-helically templated chromophores leads to increased networks for charge transport without post processing. This is a proof of concept that bioinspired, bottom-up self-assembly can be used to enhance the efficiency of organic electronic devices.

■ ASSOCIATED CONTENT

Supporting Information. Complete experimental procedures and compound characterization, solubility data, additional CD data, additional TEM data, DLS data, device protocols, and complete list of device conditions tested, AFM data, OFET current−voltage data, ^{1}H and ^{13}C NMR spectra. This material is available free of charge via the Internet at http://pubs.acs.org.

■ AUTHOR INFORMATION

Corresponding Author
E-mail: rohan.kumar@csiro.au

■ ACKNOWLEDGMENT

The authors would like to thank the Commonwealth Scientific and Industrial Research Organization, Australia and the Victorian Organic Solar Cell Consortium for generous support. Additionally, we would like to thank Dr. Carl Braybrook, Dr. Mark Bown, Dr. Jo Cosgriff, Dr. Mike Devery, Mr. Tino Ehlig, Dr. James Mardell, Dr. Roger Mulder, Dr. Scott Watkins, Dr. Richard Williams, and Dr. Doojin Vak for technical assistance. We thank a reviewer for drawing our attention to the possibility of an excitonically coupled conformation of chromophores existing within the α-helical secondary structure.

■ REFERENCES

(1) (a) Lehn, J.-M. *Chem. Soc. Rev.* **2007**, *36*, 151–160. (b) Whitesides, G. M.; Mathias, J. P.; Seto, C. T. *Science* **1991**, *254*, 1312–1319.

(2) (a) Seeman, N. C. *Nature* **2003**, *421*, 427–431. (b) Gothelf, K. V.; LaBean, T. H. *Org. Biomol. Chem.* **2005**, *3*, 4023–4037.

(3) (a) Chworos, A.; Severcan, I.; Koyfman, A. Y.; Weinkam, P.; Oroudjev, E.; Hansma, H. G.; Jaeger, L. *Science* **2004**, *306*, 2068–2072. (b) Leontis, N. B.; Lescoute, A.; Westhof, E. *Curr. Opin. Struct. Biol.* **2006**, *16*, 279–287. (c) Severcan, I.; Geary, C.; Verzemnieks, E.; Chworos, A.; Jaeger, L. *Nano Lett.* **2009**, *9*, 1270–1277.

(4) (a) Gazit, E. *Chem. Soc. Rev.* **2007**, *36*, 1263–1269. (b) Reches, M.; Gazit, E. *Science* **2003**, *300*, 625–627. (c) Ghadiri, M.; Granja, J.; Milligan, R.; McRee, D.; Khazanovich, N. *Nature* **1993**, *366*, 324–327. (d) Hartgerink, J. D.; Beniash, E.; Stupp, S. I. *Science* **2001**, *294*, 1684–1688.

(5) (a) Hoeben, F. J. M.; Jonkheijm, P.; Meijer, E. W.; Schenning, A. P. H. J. *Chem. Rev.* **2005**, *105*, 1491–1546. (b) Yamamoto, Y.; Fukushima, T.; Suna, Y.; Ishii, N.; Saeki, A.; Seki, S.; Tagawa, S.; Taniguchi, M.; Kawai, T.; Aida, T. *Science* **2006**, *314*, 1761–1764. (c) Bhosale, R.; Mísek, J.; Sakai, N.; Matile, S. *Chem. Soc. Rev.* **2010**, *39*, 138–149. (d) Wasielewski, M. R. *Acc. Chem. Res.* **2009**, *42*, 1910–1921.

(6) Jatsch, A; Schillinger, E.-K.; Schmid, S.; Bäuerle, P. *J. Mater. Chem.* **2010**, *20*, 3563–3578.

(7) (a) Iwaura, R.; Hoeben, F. J. M.; Masuda, M.; Schenning, A. P. H. J.; Meijer, E. W.; Shimizu, T. *J. Am. Chem. Soc.* **2006**, *128*, 13298–13304. (b) Alesi, S.; Brancolini, G.; Melucci, M.; Capobianco, M. L.; Venturini, A.; Camaioni, N.; Barbarella, G. *Chem.—Eur. J.* **2008**, *14*, 513–521. (c) Spada, G. P.; Lena, S.; Masiero, S.; Pieraccini, S.; Surin, M.; Samor, P. *Adv. Mater.* **2008**, *20*, 2433–2438. (d) Jatsch, A.; Kopyshev, A.; Mena-Osteritz, E.; Bäuerle, P. *Org. Lett.* **2008**, *10*, 961–964. (e) Janssen, P. G. A.; Meeuwenoord, N.; van der Marel, G.; Jabbari-Farouji, S.; van der Schoot, P.; Surin, M.; Tomović, Z.; Meijer, E. W.; Schenning, A. P. H. J. *Chem. Commun.* **2010**, *46*, 109–111.

(8) Schmid, S.; Mena-Osteritz, E.; Kopyshev, A.; Bäuerle, P. *Org. Lett.* **2009**, *11*, 5098–5101.

(9) Kawano, S.-I.; Fujita, N.; Shinkai, S. *Chem.—Eur. J.* **2005**, *11*, 4735–4742.

(10) (a) Stone, D. A.; Hsu, L.; Stupp, S. I. *Soft Matter* **2009**, *5*, 1990–1993. (b) Tsai, W.; Li, L.; Cui, H.; Jiang, H.; Stupp, S. I. *Tetrahedron* **2008**, *64*, 8504–8514. (c) Shao, H.; Nguyen, T.; Romano, N. C.; Modarelli, D. A.; Parquette, J. R. *J. Am. Chem. Soc.* **2009**, *131*, 16374–16376. (d) Schillinger, E.-K.; Mena-Osteritz, E.; Hentschel, J.; Börner, H. G.; Bäuerle, P. *Adv. Mater.* **2009**, *21*, 1562–1567. (e) Matmour, R.; De Cat, I.; George, S. J.; Adriaens, W.; Leclère, P.; Bomans, P. H. H.; Sommerdijk, N. A. J. M.; Gielen, J. C.; Christianen, P. C. M.; Heldens, J. T.; van Hest, J. C. M.; Löwik, D. W. P. M.; De Feyter, S.; Meijer, E. W.; Schenning, A. P. H. J. *J. Am. Chem. Soc.* **2008**, *130*, 14576–14583. (f) Klok, H.-A.; Rösler, A.; Götz, G.; Mena-Osteritz, E.; Bäuerle, P. *Org. Biomol. Chem.* **2004**, *2*, 3541–3544. (g) Vadehra, G. S.; Wall, B. D.; Diegelmann, S. R.; Tovar, J. D. *Chem. Commun.* **2010**, *46*, 3947–3949. (h) Channon, K. J.; Devlin, G. L.; MacPhee, C. E. *J. Am. Chem. Soc.* **2009**, *131*, 12520–12521. (i) Hasobe, T.; Saito, K.; Kamat, P. V.; Troiani, V.; Qiu, H.; Solladié, N.; Kim, K. S.; Park, J. K.; Kim, D.; D'Souza, F.; Fukuzumi, S. *J. Mater. Chem.* **2007**, *17*, 4160–4170. (j) Thünemann, A. F.; Kubowicz, S.; Burger, C.; Watson, M. D.; Tchebotareva, N.; Müllen, K. *J. Am. Chem. Soc.* **2003**, *125*, 352–356.

(11) (a) Schenning, A. P. H. J.; Meijer, E. W. *Chem. Commun.* **2005**, 3245–3258. (b) Wolffs, M.; George, S. J.; Tomović, Z.; Meskers, S. C. J.; Schenning, A. P. H. J.; Meijer, E. W. *Angew. Chem., Int. Ed.* **2007**, *46*, 8203–8205. (c) Jonkheijm, P.; van Der Schoot, P.; Schenning, A. P. H. J.; Meijer, E. W. *Science* **2006**, *313*, 80–83.

(12) (a) Tsai, W.-W.; Tevis, I. D.; Tayi, A. S.; Cui, H.; Stupp, S. I. *J. Phys. Chem. B* **2010**, *114*, 14778–14786. (b) Prasanthkumar, S.; Saeki, A.; Seki, S.; Ajayaghosh, A. *J. Am. Chem. Soc.* **2010**, *132*, 8807–8809. (c) Prasanthkumar, S.; Gopal, A.; Ajayaghosh, A. *J. Am. Chem. Soc.* **2010**, *132*, 13206–13207.

(13) Kas, O. Y.; Charati, M. B.; Rothberg, L. J.; Galvin, M. E.; Kiick, K. L. *J. Mater. Chem.* **2008**, *18*, 3847–3854.

(14) (a) Fedorova, A.; Chaudhari, A.; Ogawa, M. Y. *J. Am. Chem. Soc.* **2003**, *125*, 357–362. (b) Jones, G., II; Zhou, X.; Vullev, V. I. *Photochem. Photobiol. Sci.* **2003**, *2*, 1080–1087.

(15) Tokarski, Z.; Natarajan, L. V.; Epling, B. L.; Cooper, T. M.; Hussong, K. L.; Grinstead, T. M.; Adams, W. W. *Chem. Mater.* **1994**, *6*, 2063–2069.

(16) Barrau, S.; Zhang, F.; Herland, a; Mammo, W.; Andersson, M. R.; Inganäs, O. *Appl. Phys. Lett.* **2008**, *93*, 023307.

(17) Bradbury, J. H.; Holtzer, A. M. *J. Am. Chem. Soc.* **1956**, *78*, 947–954.

(18) (a) Tadmor, R.; Khalfin, R. L.; Cohen, Y. *Langmuir* **2002**, *18*, 7146–7150. (b) Papadopoulos, P.; Floudas, G.; Klok, H.-A.; Schnell, I.; Pakula, T. *Biomacromolecules* **2003**, *5*, 81–91.

(19) Tohyama, K.; Miller, W. G. *Nature* **1981**, *289*, 813–814.

(20) (a) Thompson, B. C.; Fréchet, J. M. J. *Angew. Chem., Int. Ed.* **2008**, *47*, 58–77. (b) Sariciftci, N. S.; Smilowitz, L.; Heeger, A. J.; Wudl, F. *Science* **1992**, *258*, 1474–1476. (c) Halls, J. J. M.; Walsh, C. A.; Greenham, N. C.; Marseglia, E. A.; Friend, R. H.; Moratti, S. C.; Holmes, A. B. *Nature* **1995**, *376*, 498–500.

(21) Wicklein, A.; Ghosh, S.; Sommer, M.; Würthner, F.; Thelakkat, M. *ACS Nano* **2009**, *3*, 1107–1114.

(22) Kagan, J.; Arora, S. K. *J. Org. Chem.* **1983**, *48*, 4317–4320.

(23) (a) Huisgen, R.; Knorr, R.; Möbius, L.; Szeimies, G. *Chem. Ber.* **1965**, *98*, 4014–4021. (b) Rostovtsev, V. V.; Green, L. G.; Fokin, V. V.; Sharpless, K. B. *Angew. Chem., Int. Ed.* **2002**, *41*, 2596–2599.

(24) Thibault, R. J.; Takizawa, K.; Lowenheilm, P.; Helms, B.; Mynar, J. L.; Fréchet, J. M. J.; Hawker, C. J. *J. Am. Chem. Soc.* **2006**, *128*, 12084–12085.

(25) Smith, K.; Barratt, M. L. *J. Org. Chem.* **2007**, *72*, 1031–1034.

(26) Kramer, J. R.; Deming, T. J. *Biomacromolecules.* **2010**, *11*, 3668–3672.

(27) Lu, H.; Cheng, J. *J. Am. Chem. Soc.* **2007**, *129*, 14114–14115.

(28) McCullough, R. D.; Lowe, R. D.; Jayaraman, M.; Anderson, D. L. *J. Org. Chem.* **1993**, *58*, 904–912.

(29) Kirihata, H; Uda, M. *Rev. Sci. Instrum.* **1981**, *52*, 68–70.

(30) (a) Míšek, J.; Vargas Jentzsch, A.; Sakurai, S. I.; Emery, D.; Mareda, J.; Matile, S. *Angew. Chem., Int. Ed. Engl.* **2010**, *49*, 7680–7683. (b) A reviewer indicated that the commonly used value of −4.8 eV for ferrocene may be in error and −5.0 eV the correct value. We have used the value of −4.8 eV to give values that relate to the majority of those in the literature.

(31) Huang, C. Y.; Klemke, J. W.; Getahun, Z.; DeGrado, W. F.; Gai, F. *J. Am. Chem. Soc.* **2001**, *123*, 9235–9238.

(32) Bradbury, J. H.; Fenn, M. D. *Aust. J. Chem.* **1968**, *36*, 231–246.

(33) Cierpicki, T.; Otlewski, J. *J. Biomol. NMR* **2001**, *21*, 249–61.

(34) (a) Langeveld-Voss, B. M. W.; Beljonne, D.; Shuai, Z.; Janssen, R. A. J.; Meskers, S. C. J.; Meijer, E. W.; Brédas, J. L. *Adv. Mater.* **1998**, *10*, 1343–1348.

(35) (a) Kreyes, A.; Amirkhani, M.; Lieberwirth, I.; Mauer, R.; Laquai, F.; Landfester, K.; Ziener, U. *Chem. Mater.* **2010**, *22*, 6453–6458. (b) Faied, K.; Frechette, M.; Ranger, M.; Mazerolle, L.; Levesque, I.; Leclerc, M.; Chen, T.-A.; Rieke, R. D. *Chem. Mater.* **1995**, *7*, 1390–1396. (c) Roux, C.; Leclerc, M. *Chem. Mater.* **1994**, *6*, 620–624.

(36) Smulders, M. M. J.; Nieuwenhuizen, M. M. L.; de Greef, T. F. A.; van der Schoot, P.; Schenning, A. P. H. J.; Meijer, E. W. *Chem.—Eur. J.* **2010**, *16*, 362–367.

(37) (a) Williams, S.; Causgrove, T. P.; Gilmanshin, R.; Fang, K. S.; Callender, R. H.; Woodruff, W. H.; Dyer, R. B. *Biochemistry* **1996**, *35*, 691–697. (b) Thompson, P. A; Muñoz, V.; Jas, G. S.; Henry, E. R.; Eaton, W. A; Hofrichter, J. *J. Phys. Chem. B* **2000**, *104*, 378–389.

(38) Maturová, K.; van Bavel, S. S.; Wienk, M. M.; Janssen, R. A. J.; Kemerink, M. *Nano Lett.* **2009**, *9*, 3032–3037.